Solar selective absorbers based on Al_2O_3:W cermets and AlSiN/AlSiON layers

L. Rebouta[1*], A. Sousa[1], P. Capela[1], M. Andritschky[1], P. Santilli[2], A. Matilainen[2], K. Pischow[2], N. P. Barradas[3], E. Alves[4]

1 Centre of Physics, University of Minho, Alameda da Universidade, 4804-533 Guimarães, Portugal

2 Savo Solar Oy, Insinöörinkatu 7, 50100 Mikkeli, Finland

3 C2TN, Instituto Superior Técnico, Universidade de Lisboa, E.N. 10, 2695-066 Bobadela, Portugal

4 IPFN, Instituto Superior Técnico, Av. Rovisco Pais, 1049-001, Lisboa, Portugal

* Corresponding author: Tel.: +351 253510472; fax: +351 253510461, e-*mail address*: rebouta@fisica.uminho.pt

Abstract

Solar selective coatings based on double Al_2O_3:W cermet layers and AlSiN/AlSiON bilayer structures were prepared by magnetron sputtering. Both were deposited on stainless steel substrates using a metallic tungsten (W) layer as back reflector. The coating stacks were completed by an antireflection (AR) layer composed of Al_2O_3, SiO_2, or $AlSiO_x$. Spectrophotometer measurements, X-Ray diffraction, Scanning electron microscopy, Energy Dispersive X-Ray Spectroscopy and Rutherford Backscattering Spectrometry were used to characterize the optical properties, crystalline structure, morphology and composition of these coatings. The spectral optical constants of the single layers were calculated from the reflectance and transmittance measurements and used to design the optical stack. The coatings exhibit a solar absorptance of 93%-95% and an emissivity of 7%-10% (at 400 ºC). The coatings also exhibit excellent thermal stability, with small changes in the optical properties of the coating during heat-treatments at 400 ºC in air for 2500 h and at 580 ºC in vacuum for 850 h. The coating based on the AlSiN/AlSiON bilayer structure was obtained with an Al:Si ratio of 2.5:1. These coatings revealed similar performance as the one obtained with coatings based on Al_2O_3:W cermet layers.

Keywords: AlSiN/AlSiON; Al_2O_3:W cermet; solar selective absorber, dielectric function modelling; optical constants, thermal emittance

1. Introduction

Absorbers for photo-thermal conversion have already been developed for decades [1-4]. They are commonly used for water heating systems (T<150 ºC). The concentrated solar power (CSP) technology allows the electricity production in large-scale plants. One of the CSP technologies is based on parabolic-trough systems [5, 6], where the energy is absorbed in a solar

selective coating deposited onto the absorption tube, which reaches high temperatures (up to 400 ºC in mid-temperature applications). The efficiency of this technology can be increased, e.g. by increase of the solar absorptance and decrease of emissivity (improving the optical and thermal properties) of the selective coating, and by increasing the operating temperature (>450 °C). Elevated working temperatures for a prolonged period require an excellent thermal stability of the materials used for the receiver tube. Hence, the focus is not only on the optical properties of the receiver tube, but also on the long term (>20 y) durability and oxidation resistance of the solar selective coating.

Several materials have the appropriate optical properties and can have the necessary durability at operating temperatures at 400^{o}C and above, and potential materials have been identified in the review performed by Kennedy [7]. Various binary and ternary metal compounds satisfy these requirements, particularly those formed from the refractory metals of groups 4, 5 and 6. For example, the titanium, zirconium, or hafnium metal boride, carbide, oxide, nitride, and silicide materials have some of the highest melting points in nature, and some of them also have a good oxidation and corrosion resistance.

A very high solar absorption can be achieved when the coating has a graded refractive index n and extinction coefficient k. Both parameters should be highest at the metal/substrate interface (infrared reflector), and then gradually decrease towards the surface. This can be easily done with a ceramic-metal composite coating (cermet) [8, 9] by decreasing continuously the metal volume fraction from the interface metal/substrate to the surface. The cermet consists of small metal particles embedded in a ceramic matrix, where the role of the metallic particles is to increase the solar absorption, due to the interband transitions in the metal, and to reduce the absorption in the thermal IR region due to the small particle size. The concept offers a broad range of options for solar selectivity optimization and it depends on the proper choice of constituents, coating thickness, particle concentration, size, shape, and orientation. Al_2O_3, SiO_2, ZrO_2 and AlN have been used as matrix, because they are ceramics with stability at high temperatures, together with metals inclusions, such as W, Ag, Ni, Pt, Mo [7-14], which are some of the metals with relatively good oxidation resistance.

Instead of the graded refractive index and extinction coefficient, a bilayer structure can be used, where the solar absorptance is optimized through the interference effect [15-17]. These multilayer interference stacks with adequate materials can also have high solar absorption, low thermal emittance, and be stable at elevated temperatures (≥ 350ºC). The optical constants and thicknesses of different layers should be chosen in order to produce a cancellation between light reflected from the top surface and from the first interface, and between light reflected in the first interface and in the second interface, and so on. An optical path length of 1/4 wavelength (in a

layer) would produce a net shift of 1/2 wavelength between the mentioned reflections, resulting in cancellation. In order to enhance the solar absorption, this removal should occur for wavelengths in the solar radiation spectrum. For a medium with constant refractive index, *n*, the optical path length can be calculated as the product of the refractive index with the physical length, *d*, *nd*. The refractive indexes and physical thicknesses of the bilayer structure should be chosen in order to obtain destructive interference at wavelengths around 0.5 μm and 1.5 μm, contributing to the decrease of the reflectance in these regions.

This solution was used in both cases, and we employed two distinctive layers, High Absorbing layer (HA) and Low Absorbing layer (LA), with decreasing n and k for the absorption of the solar radiation. This design can be done with cermets, where the metal volume fraction is used to adjust the refractive index of each layer, or with other materials with adequate refractive index and extinction coefficient [18-20].

AlSiON is known for its high thermal stability and its exceptional corrosion resistance [21, 22]. AlSiN also has good thermal and chemical stability, and the optical properties of both can be tuned by changing their composition [23]. Additionally, AlSiN/AlSiON multilayers provide a better manufacturability in a continuous large-scale production, where only one target is needed. In this work, two different thermal solar selective coating stacks were developed, one based on Al_2O_3:W cermets and, as an alternative concept, another based on AlSiN/AlSiON ceramic layers.

The entire coating stack was completed by a pure metallic tungsten (W) layer at the substrate coating interface to provide high reflectivity (and low emissivity) in the infrared region (IR), and a Al_2O_3, SiO_2 or $AlSiO_x$ layer as antireflection (AR) layer on the outside. The AR layer and the W layer also serve as diffusion barriers. The AR layer decreases the diffusion of oxygen and other contaminants from the surrounding atmosphere towards the coating, and the W layer decreases the diffusion from the stainless steel substrate into the coating. The optical design of multilayered coatings was performed through the spectral optical constants of the single layers, and in this work was used the modelling software SCOUT [24].

2. Experimental details

2.1 Sample preparation and characterization

The W metallic layer was deposited from a pure metal tungsten target by DC magnetron sputtering and in static mode. Experimental details are shown in table 1. Prior to the deposition, the vacuum chamber was evacuated to a base pressure of $2x10^{-4}$ Pa, and during the deposition a pulsed bias of -60 V (frequency 90 kHz) was applied to the substrate holder.

Al_2O_3:W cermets were deposited by simultaneous sputtering from two pure metal W and Al circular targets (diameter 4 inch), which were placed horizontally. The substrate holder rotated with a constant speed (15 rpm) over the targets. Al_2O_3:W cermets with varying W content were obtained by maintaining constant the Al target sputter current (0.5 A) as well as the O_2 flow, but varying the current applied to the W target (0.1 A – 0.8 A). The AR layer based on Al_2O_3 was prepared in rotation mode, as the Al_2O_3:W layers, under an Ar/O_2 atmosphere and employing only the Al target.

AlSiN and AlSiON were deposited by reactive DC sputtering in static mode from an Al target with 9 Si discs (diameter 1 cm) located in the erosion zone in an atmosphere containing oxygen, nitrogen and argon. HA layers were produced employing solely nitrogen as a reactive gas (AlSi nitride) and the LA layers were based on AlSi-oxynitrides. The AR layer based on $AlSiO_x$ thin films was also prepared under an Ar/O_2 atmosphere. Two coatings were optimized with this target , one with layers deposited in static mode and another with layers deposited in rotation mode.

The SiO_2 layer was deposited by Plasma Enhanced Chemical Vapour Deposition (PECVD) with the help of an Inductively Coupled Plasma (ICP) source using Octamethylcyclotetrasiloxane (OMCTS), $((CH_3)_2SiO)_4$ as a precursor. During those depositions a rf power of 3000 W, an oxygen flow of 750 sccm and precursor flow of 15 g/h were used. The total pressure during deposition was 0.4 Pa.

The structural properties of the films were studied by X-ray diffraction (XRD) employing a Bruker AXS Discover D8 operating with $Cu_{K\alpha}$ radiation. X-Ray diffraction measurements have been performed for an angle of incidence of 3º. Energy Dispersive X-Ray Spectroscopy (EDS) analysis and Rutherford backscattering Spectrometry (RBS) measurements were used to evaluate the composition of the thin films. EDS was performed with the electron beam of the scanning electron microscope with a EDAX- Pegasus X4M system and an energy of 13.5 keV and RBS measurements were performed with a proton beam with energy of 2.3 MeV, at an angle of incidence of 0º. The scanning electron microscope used in the study was a FEI Nova NanoSEM 200. Optical measurements, in transmittance and reflectance modes, were performed in the wavelength range of 250-2500 nm, using a Shimadzu spectrometer. The total reflectance measurements were performed with an incidence angle of 8º using an integrating sphere attachment. The normal solar absorptance, α_s, is defined as a weighted fraction between absorbed radiation and incoming solar radiation, and it was determined using the calculated or experimentally obtained spectral reflectance data $R(\lambda)$ and ASTM AM1.5D solar spectral irradiance, $I_s(\lambda)$, according to [2]:

$$\alpha_s = \frac{\int_{0.3\mu m}^{2.5\mu m} I_s(\lambda)[1 - R(\lambda)]d\lambda}{\int_{0.3\mu m}^{2.5\mu m} I_s(\lambda)d\lambda} \quad \text{(eq. 1)}$$

The absorptance calculations were made over the portion of the electromagnetic spectrum from 0.3 to 2.5 μm.

A Fourier Transform Infrared (FTIR) spectrophotometer from Agilent Technologies was used to measure the spectral reflectance in the infrared wavelength range, 1.6-16.7 μm, which is equipped with an integrating sphere. The normal thermal emittance, ε_{th}, is a weighted fraction between emitted radiation and the Planck blackbody distribution and, at a specific temperature T was calculated from [2]:

$$\varepsilon_{th} = \frac{\int_{1.6\,\mu m}^{25\mu m} I_{bb}(\lambda)[1 - R(\lambda)]d\lambda}{\int_{1.6\,\mu m}^{25\mu m} I_{bb}(\lambda)d\lambda} \quad \text{(eq. 2)}$$

where $I_{bb}(\lambda)$ is the spectral blackbody emissive power and $R(\lambda)$ the spectral reflectance. For reflectance measurements it was used, as a reference, a gold thin film. Considering the gold has an absolute reflectance lower than 100 %, the reflectance of a copper plate was multiplied by a constant factor (lower than 1) in order to obtain a thermal emittance of 3%. All IR reflectance measurements were subjected to the same correction. The thermal emittance was also measured with an emissometer AE-AD3 from Devices & Service Company (at 80 ºC) and within the error of the measurement (± 1%) the results for 80 ºC obtained from the two measurements are similar.

The solar selective absorber coating was developed using the following steps:

(i) Preparation of single sheets. which correspond to several layers with different metal volume fraction in the case of Al_2O_3:W cermets, films with different content of nitrogen and oxygen in the case of AlSiN and AlSiON, the back reflector, W; and the antireflection layers, Al_2O_3, $AlSiO_x$ and SiO_2;

(ii) optical characterization of individual layers deposited on glass substrates. The transmittance (T) and reflectance (R) of films can be used to obtain the optical constants. The bands in the optical spectra can be described by the classical theory of the optical propagation, where light is treated as electromagnetic waves and atoms or molecules are modeled as classical dipole oscillators, which enables the calculation the frequency dependence of the complex dielectric constant and the dependence of the absorption coefficient and refractive index [26, 27]. The experimental curves of T and R were modelled with SCOUT [24]. From the modelling the coating thickness was obtained (and deposition rate) , as well as the spectral optical constants (n and k) as a function of the wavelength λ.

(iii) With spectral optical constants of different materials, it is possible to build the optical spectra (T and R) of a multilayer, and the SCOUT software was used to design a four layer coating stack with optimized absorptance α_s and emissivity ε_{th}. This modelling step allows selecting the materials to be used and respective thicknesses.

(iv) Finally, the multilayered coating was deposited onto a polished stainless steel substrate, using the materials and thicknesses selected in the modelling step.

3. Experimental Results

3.1 Single layers

A tungsten layer was chosen as back reflector. This layer improves significantly the reflectance of polished (R_{RMS} < 0.2 μm) stainless steel to about 96 % at λ > 2500nm (Fig 1a). According to the Kirchoff law, the increased reflectance decreases emissivity from ε = 14% (SS substrate) to ε = 4% (at 80 ºC). Fig.1b also presents the spectral optical constants of W layer.

Fig. 2 shows n = f(λ) and k = f(λ) for the eight HA and LA layers, as obtained from the numerical simulation of the Transmittance and Reflection measurements of the single Al_2O_3:W cermet layers on glass with the SCOUT software. The simulation requires a model for the dielectric function. Firstly we tried the use of an effective dielectric function for the two phase composite (W and Al_2O_3) based on the dielectric functions obtained for the single layers of the respective materials based on models of Maxwell Garnett [28] or Bruggeman [29]. Neither of the models gave satisfactory results. A partial oxidation of tungsten is expected, which means that the Al_2O_3:W films are not a pure two phase composite. The use of a one phase model, which assumes an isotropic medium, gave good results and allowed the optical characterization of the individual layers and subsequent multilayer design. The dielectric function ($\tilde{\varepsilon}$) was considered as a sum of several contributions, which model intraband and interband transitions:

$$\tilde{\varepsilon}_r = \tilde{\varepsilon}_{background} + \tilde{\varepsilon}_{Drude} + \sum \tilde{\varepsilon}_{Lorentz} + \tilde{\varepsilon}_{OJL} \qquad \text{(eq. 3)}$$

Where, $\tilde{\varepsilon}_{background}$, represents a background, $\tilde{\varepsilon}_{Drude}$, a Drude term, representing unbound electron oscillators, which describe the intraband transitions of the electrons in the conduction band, $\tilde{\varepsilon}_{Lorentz}$, a Lorentz term representing the bound harmonic oscillators [30], which was used to describe the interband transitions into the upper half of the conduction band, and $\tilde{\varepsilon}_{OJL}$, the OJL term [31], used to describe the band gap transitions. This term follows the model proposed by O'Leary, Johnson and Lim [31], and parabolic bands are assumed with tail states exponentially decaying into the band gap. The fit parameters of the OJL interband transition model are the gap energy, E_0, the tail state exponent of the valence band, γ, and the overall strength of the

transition. The combination of these interactions gave a satisfactory simulation of the experimental dielectric function of single layers. The aluminium oxide layer presents a refractive index around 1.7, which increases with the W content, as expected due to the increase of the metallic character. , The HA layer was selected from the group made with high W current value, and the LA layer was obtained from those prepared with small W current. The findings apply to the AlSiN and AlSiON layers on glass where a similar approach was used to simulate the dielectric function, the first as HA layer and the second as LA layer. In this case, the nitrogen and oxygen content were varied to tune the optical properties. Nitrides with low N contents have high refractive index and extinction coefficient. On the other hand, an increase of the nitrogen content leads to an decrease of these parameters.

The composition of single Al_2O_3:W layers, deposited on Cu foil was analyzed by RBS as shown in Fig. 3. The RBS spectra suggest an O/Al ratio of 1.5. Similar compositions were obtained by EDS. The structures of the different layers analyzed are indicated in table 1.

The single layers used to build the absorber coating (HA and LA layers) were also deposited with thicknesses between 700 and 900 nm and analyzed by XRD. The results are shown in Fig.4, where the XRD patterns of Al_2O_3:W cermet layers, deposited on polished stainless steel, are shown in Fig. 4a and the XRD patterns of AlSiN and AlSiON layers, deposited on glass, are shown in Fig.4b. The XRD measurements were performed with an incidence angle of 3º, and in all cases a broad peak is present. In Al_2O_3:W layers (Fig. 4a) the broad peak is around $2\theta=40º$, which could be assigned to (110) planes of bcc W lattice. The intensity of the broad peak increased with tungsten volume fraction (f), but the FWHM of about 7º, indicates that both, W and Al_2O_3, are amorphous. The other peaks, referred by S, correspond to the stainless steel substrate. The broad peak present in the diffractograms of the AlSiN and AlSiON layers (Fig. 4b) is the same seen for glass substrates, which indicates those layers are XRD amorphous.

3.2 Multilayers

Four multilayer stacks were built using a polished stainless steel substrate, a back reflector (W), a double-cermet film structure (CM1 and CM2) or an AlSiN high absorption layer together with an AlSiON low absorption layer (SAON1 and SAON2 multilayers) and an antireflection layer (Al_2O_3 on CM2, SiO_2 on CM1 and SAON1 and $AlSiO_x$ on SAON2). SAON1 individual layers were deposited in static mode, while SAON2 single layers were deposited in rotation mode. Sketches of these multilayers are shown in Fig 5, where CM1 and CM2 multilayers, are those based on AlO3:W cermets and the SAON1 and SAON2 are based on AlSiN/AlSiON bilayers. In each sketch the individual layers used in each multilayer stack and their thicknesses

are described. The stacks were deposited on stainless steel substrates without breaking the vacuum, adjusting the deposition time for the individual layers in order to obtain the thickness values coming from the numerical stack simulation. The SiO_2 layer was deposited in another chamber, which means that, in these cases the vacuum was broken after the deposition of the first three layers.. In Fig. 6 the total reflectance of the four stacks CM1, CM2, SAON1 and SAON2 is shown. CM2 and SAON1 are thinner than CM1 and SAON2, respectively, and that shifts the step on the wavelength scale to lower wavelengths, which has a strong effect in the emissivity values. CM2 has lower absorptance (92.5 %) but also significantly lower thermal emittance at 400 ºC (7 %). SAON1 and SAON2 present an absorptance of 94 % and a thermal emittance of 8 % and 9 % (at 400 ºC), respectively.

SEM images of CM1 and SAON1 are shown in Fig.7a and 7b, respectively. In both stacks, the first layer (W layer) shows a morphology that suggests a columnar growth (XRD analysis reveals they are polycrystalline). The top layer (AR layer) shows a featureless morphology (XRD analyses show an amorphous layer). The layers between the AR layer and the W layer, as shown in Fig. 7, are almost featureless, and XRD does not show any additional peaks. The contrast between the two different cermet layers and between the AlSiN and AlSiON layers is very small, and it is not resolved in the SEM pictures. The thickness of the intermediate layer shown in the SEM pictures corresponds to the double layer structure, being the 126 nm layer from CM1 absorber coating (Fig. 7a), which corresponds to the sum of the thicknesses of HA+LA layers indicated in Fig. 5 (68+47 nm), while for SAON1, the 84 nm layer (Fig.7b) corresponds to the layers with 46 and 42 nm. All layers of the SAON1 coating have thicknesses slightly lower than expected, but this can be justified by the tilt of the sample during the SEM characterization.

3.3 Oxidation resistance and thermal stability

The thermal stability was evaluated with thermal treatments in air at 400 ºC and vacuum at 580 ºC. Fig. 8 represents the reflectance of coating CM1 as deposited and after thermal annealing at 400 ºC in air (Fig. 8a) and at 580 ºC in vacuum (Fig. 8b). The solar absorptance and thermal emittance (at 400 ºC) after each step are indicated in the legend of the figure. Thermal annealing of CM1 induced a shift of the step on the reflectance to lower wavelengths. This shift resulted in a decrease of both solar absorptance and thermal emittance. However, in both cases a change is seen after the first step, and only minor changes occur after further steps. For example, the shift is visible after 432 h at 400 ºC in air, but additional 2000 h in the same conditions did not induce further changes (Fig. 8a). All intermediate steps (not shown) have a profile similar to that

obtained for 432 h. This initial shift was not seen in coating CM2, (Fig. 9a), where the spectral reflectance did not change after 2496 h at 400 ºC in air and solar absorptance and thermal emittance remained practically unchanged. CM2 has an Al_2O_3 layer as antireflection coating, while the CM1 coating has a SiO_2 layer prepared by PECVD. SAON1 and SAON2 showed a similar behavior, when compared with CM1 and CM2, and again SAON1 has a SiO_2 layer prepared by PECVD as AR layer while SAON2 (Fig. 9b) has an $AlSiO_x$ layer developed by magnetron sputtering. The IR reflectance for $\lambda > 4$ μm did not decrease, which shows that the high reflectivity of the W back reflector remained unchanged, indicating that the W layer did not oxidize.

In Fig.10, the XRD patterns of CM1 and SAON1 samples are shown as measured in the as deposited state and after thermal treatments. The measurements were performed with a fixed grazing incidence of 3º. The peak located at 40.0º corresponds to (110) planes of W bcc structure. The peaks referenced by S correspond to the stainless steel substrate. These results show that the W layer is polycrystalline, while the other layers are X-Ray amorphous (see also Fig. 4). After the thermal treatments a very small decrease in the peak-width of the W layer and of the stainless steel substrate can be noted, and the other layers continue X-Ray amorphous. The grain growth in the tungsten polycrystalline layer is expected. The grain boundaries have an excess of energy and the minimization of energy drives the process of grain growth. The increase of temperature increases the boundary mobility and thus facilitates the grain growth [32, 33]. The other layers did not reveal any grain growth, which also shows its good thermal stability. The reduction of the total interfacial energy provides the driving force of grain growth.

4. Discussion

Multilayer stacks based on Al_2O_3:W cermets together with a W back reflection layer and an Al_2O_3 or SiO_2 AR layer may form a very effective selective solar absorbing [13]. A similar solution can be obtained by a combination of aluminium rich AlSi nitride with an AlSi-oxynitride, both with a W reflection layer between the absorbing stack and the substrate and an $AlSiO_x$ or SiO_2 anti-reflection layer. Optical properties (α_s and ε_{th}) of these multilayer stacks are similar to several other stacks proposed in the literature for selective solar thermal absorption coatings. Different values of solar absorptance and thermal emittance for coatings of the same type, as seen in Fig.8, are related with target diameter (4 inches). This leads to a small region where the film thickness is homogeneous, and samples located in different positions in the substrate holder can have small changes in the layer thicknesses. Nevertheless, the long-term resistance at elevated temperatures in air and in vacuum indicate that the solution based on AlSiN/AlSiON bilayers is a very stable coating. During a high-temperature treatment in air at

400^{o}C, α_s and ε_s remain unchanged. For comparison, the solar absorptance of the different coatings as a function of the annealing time is shown in Fig. 11 for both types of annealing. As already seen from Fig.8 and 9, CM2 and SAON2 maintain their optical performance at 400 ºC in air (Fig. 11a), while CM1 and SAON1 showed an initial change in the first step, but the solar absorptance was maintained for further annealing steps. However, after the thermal annealing at 580 ºC in vacuum (<1x10^{-3} Pa), CM1 revealed a slightly better performance than SAON1 and SAON2 (Fig.11b). The solar absorptance of sample CM1 remained basically unchanged, and it decreased slightly in SAON1 and SAON2. The IR reflectance was only measured in the as deposited samples and after all thermal treatment steps. The CM1 sample revealed a small decrease in emissivity, while, for other samples, the emissivity remained unchanged or had a slight increase. The decrease in emissivity is mainly due to the oxidation of SiO_x AR layer, which shifts the step on the reflectance to lower wavelengths. The SiO_x AR layer was prepared by PECVD and it is not fully oxidized. IR transmittance measurements (not shown) also showed the presence of some water molecules. A single layer was thermal annealed at 300 ºC in air and showed some optical changes after 24 h, but then remained unchanged after much longer anneal times. These changes can be associated with oxidation and water vapour release.

The AR layer, together with the LA cermet or AlSiON layers, respectively retard oxygen penetration sufficiently to prevent the HA layer and W oxidation. As the solar absorptance remained almost unchanged, we can conclude that the LA cermet or AlSiON layers, although not fully stoichiometric, do not react with the oxygen or other potential contaminants in the air. We can obtain a similar conclusion from the emissivity behaviour. ε_s is very sensitive to an eventual oxidation of the W layer. Measurements on pure W [34] indicate an oxidation rate on air at 400^{o}C which would lead to a complete loss of the W-layer in the 1500 h timeframe. The coating design of the three outer layers was performed in order to maximize the absorptance in the solar radiation range, but to be transparent to longer wavelengths. As this infrared radiation is reflected on the tungsten layer, its oxidation would change the reflectivity properties and thus the emissivity. (eq. 2). Thus, the constant ε_s indicate that no perceptible oxidation of the W occurs.

X-ray diffraction results indicate a very minor change in the average grain size of the W-layer. With these results it is possible to conclude that no significant amounts of contaminants diffuse from the stainless steel substrate to the absorbing layers. An appreciable amount of those contaminants would cause a decrease of the reflectivity of the W layer, which would lead to an increase of the coating emissivity. In same way, the presence of those contaminants in absorbing layers would change its optical properties (or equivalently the optical constants n and k), and thus would change the solar absorptance. As seen with individual layers prepared with different reactive gas flows, a small change in the composition leads to a variation in the optical constants.

The measurements also show that the layers deposited by DC sputtering do not decompose in any way. Thus, the optical measurements are very sensitive to any changes in the coating composition and the results show that those processes do not occur.

The coating based on AlSiN/AlSiON bilayer structure was obtained with an Al:Si ratio of 2.5:1. Significantly higher Si contents apparently do not add to better performance of the material in the form of thin coatings. Higher Si content caused some difficulties in obtaining a good solution for the solar absorption α_s.

The use of different AR layers did not introduce significant changes. In terms of thermal stability, SiO_2 was used in both type of absorbing coatings with good results, as well as, Al_2O_3 on Al_2O_3:W cermets and $AlSiO_x$ on AlSiN/AlSiON based coating. However, SiO_2 has a lower refractive index than Al_2O_3 and can, therefore, be more effective for the maximization of absorptance.

5. Summary

A novel coating for selective absorption of solar radiation based on AlSiN and AlSiON layers was fabricated. The multilayer was built with a pure metallic tungsten (W) layer as a back reflector, followed by two absorption layers (HA layer and LA layer) for the absorption of the solar energy, and by an antireflection (AR) layer. The structures have been simulated by the SCOUT software using suitable dielectric function models. The AlSiN and AlSiON layers with adequate Al:Si ratio (2.5 to 1) showed good solar selective properties (solar absorptance of 94-95% and emissivity of 8-9% at 400 ºC), as well as, good thermal stability. The samples with this Al:Si ratio, after a heat treatment in air at 400 ºC during 2500 h showed an absorptance change of 1%, in average, and an emissivity variation around 0.5%. A heat treatment at 580 ºC in vacuum during 850 h promoted a solar absorptance decrease of 3%, while the emissivity increased less than 1%.

The coating based on Al_2O_3:W cermet revealed a slightly better performance than those based on AlSiN and AlSiON layers, with a similar change in the absorptance in air at 400 ºC during 2500 h, but with better performance with the thermal annealing in vacuum at 580 ºC. The small changes in the emissivity for these long heat treatments indicate that no perceptible oxidation of the W occurs. The small absorptance change is justified by a small oxidation of the outer layers. The coatings based in Al_2O_3:W cermets have been studied in the past [7, 13, 35] with good thermal stability and are good candidates to be used in the concentrated solar power applications. The coating based on AlSiN/AlSiON layers revealed a similar performance, and thus also has potential for those applications.

Acknowledgements

The authors acknowledge the funding from the Finnish Funding Agency for Technology and Innovation, Tekes, and from FEDER funds through the "Programa Operacional Factores de Competitividade – COMPETE" and from national funds by FCT- "Fundação para a Ciência e a Tecnologia", under project no. PEst-C/FIS/UI0607/2011.

References

[1] H.G. Craighead, R.A. Buhrman, "Optical-Properties of Selectively Absorbing Ni-Al_2O_3 Composite Films", Appl. Phys. Lett. 31 (1977) 423-425.

[2] B.O. Seraphin, "Chemical vapor deposition of thin semiconductor films for solar energy conversion", Thin Solid Films 39 (1976) 87–94.

[3] W.F. Bogaerts, C.M. Lampert, "Materials for photothermal solar energy conversion", J. Mater. Sci. 18 (1983) 2847-2875.

[4] G.A. Niklasson, C.G. Granqvist, "Surfaces for selective absorption of solar energy: An annotated bibliography 1955-1981", J. Mater. Sci. 18 (1983) 3475-3534.

[5] W.W. Shaner, W.S. Duff, "Solar thermal electric power systems: Comparison of line-focus collectors", Sol. Energy 22 (1979) 49-61.

[6] A. Fernández-García, E. Zarza, L. Valenzuela, M. Pérez, "Parabolic-trough solar collectors and their applications", Renew. Sustainable Energy Rev. 14 (2010) 1695–1721.

[7] Kennedy, C.E., 2002, Review of Mid- to High-Temperature Solar Selective Absorber Materials, NREL/TP-520-31267, Golden, CO: National Renewable Energy Laboratory.

[8] H.G. Craighead, R. Bartynski, R.A. Buhrman, L. Wojcik, A.J. Sievers, "Metal-Insulator Composite Selective Absorbers", Sol. Energy Mater. 1 (1979) 105-124.

[9] C.G. Granqvist, O. Hunderi, "Optical properties of Ag-SiO_2 Cermet films: A comparison of effective-medium theories", Phys. Rev. B 18 (1978) 2897-2906.

[10] G.A. Niklasson, "Optical properties of inhomogeneous two-component materials" in: Materials Science for Solar Energy Conversion Systems, ed. C.G. Granqvist, Pergamon, Oxford, 7-43 (1991).

[11] M. Farooq, M.G. Hutchins, "Optical properties of higher and lower refractive index composites in solar selective coatings", Sol. Energy Mater. Sol. Cells 71 (2002) 73–83.

[12] Qi-Chu Zhang, Y.G. Shen, "High performance W–AlN cermet solar coatings designed by modelling calculations and deposited by DC magnetron sputtering", Sol. Energy Mater. Sol. Cells 81 (2004) 25–37.

[13] A. Antonaia, A. Castaldo, M.L. Addonizio, S. Esposito, "Stability of W-Al_2O_3 cermet based solar coating for receiver tube operating at high temperature", Sol. Energy Mater. Sol. Cells 94(2010)1604–1611.

[14] F. Cao, K. McEnaney, G. Chen, Z. Ren, "A review of cermet-based spectrally selective solar absorbers", Energy Environ. Sci. 7 (2014) 1615-1627.

[15] Q.C. Zhang, D.R. Mills, "Very low-emittance solar selective surfaces using new film structures", J. Appl. Phys. 72 (1992) 3013-3021.

[16] Y. Yin, R.E. Collins, "Optimization and analysis of solar selective surfaces with continuous and multilayer profiles", J. Appl. Phys. 77 (1995) 6485-6491.

[17] M. Farooq, M.G. Hutchins, "A novel design in composites of various materials for solar selective coatings", Sol. Energy Mater. Sol. Cells 71 (2002) 523–535.

[18] H.C. Barshilia, N. Selvakumar, K.S. Rajam, "Thermal stability of TiAlN/TiAlON/Si_3N_4 tandem absorbers prepared by reactive direct current magnetron sputtering", J. Vac. Sci. Technol. A25 (2007) 383–390.

[19] Miao Du, Lei Hao, Jing Mi, Fang Lv, X. Liu, L. Jiang, S. Wang, "Optimization design of $Ti_{0.5}Al_{0.5}N/Ti_{0.25}Al_{0.75}N$/AlN coating used for solar Selective applications", Sol. Energy Mater. Sol. Cells 95 (2011) 1193-1196.

[20] L. Rebouta, A. Pitães, M. Andritschky, P. Capela, M.F. Cerqueira, A. Matilainen, K. Pischow, "Optical characterization of TiAlN/TiAlON/SiO_2 absorber for solar selective applications", Surf. Coat. Technol. 211 (2012) 41-44.

[21] T. Ekström, M. Nygren, "SiAlON Ceramics", J. Am. Ceram. Soc. 75 (1992) 259-276.

[22] G.P. Bernhardt, J.I. Krassikoff, B.T. Sturtevant, R.J. Lad, "Properties of amorphous thin films grown by RF magnetron co-sputtering", Surf. Coat. Tech. 258 (2014) 1191-1195.

[23] Guanghui Liu, Zhenzhen Zhou, Qinhua Wei, Fan Fei, Hua Yang, Qian Liu, "Preparation and tunable optical properties of ion beam sputtered SiAlON thin films", Vacuum 101 (2014) 1-5.

[24] W. Theiss, in: M. Theiss (Ed.), SCOUT Thin Film Analysis Software Handbook, Hard-and Software, Aachen, Germany, 2002.

[25] L. Rebouta, P. Capela, M. Andritschky, A. Matilainen, P. Santilli, K. Pischow , E. Alves, "Characterization of TiAlSiN/TiAlSiON/SiO_2 optical stack designed by modelling calculations for solar selective applications", Sol. Energy Mater. Sol. Cells 105 (2012) 202–207.

[26] T.C. Paulick, "Inversion of normal-incidence (R, T) measurements to obtain n + ik for thin films", Appl.Opt. 25 (1986) 562-564.

[27] M. Fox, "Optical properties of solids", Oxford University Press Inc, New York, 2001.

[28] J.C. Maxwell Garnett, "Colours in metal glasses and in metallic films", Philos. Trans. R. Soc. London 203 (1904) 385-420.

[29] D.A.G. Bruggeman, "Calculation of the various physical constants of heterogeneous constants", Ann. Phys. 24 (1935) 636-664,

[30] C.C. Kim, J.W. Garland, H. Abad, P.M. Raccah, “Modeling the optical dielectric function of semiconductors: extension of the critical-point parabolic-band approximation”, Phys. Rev. B 45 **(**1992) 11749-11767.

[31] S.K. O_Leary, S.R. Johnson, P.K. Lim, “The relationship between the distribution of electronic states and the optical absorption spectrum of an amorphous semiconductor: an empirical analysis”, J. Appl. Phys. 82 (1997) 3334-3340.

[32] S.K. Ganapathi, D.M. Owen, A.H. Chokshi, “The kinetics of grain growth in nanocrystalline copper”, Scripta Metall. et Mater. 25 (1991) 2699-2704.

[33] I. Andersen, Ø. Grong, “Analytical modelling of grain growth in metals and alloys in the presence of growing and dissolving precipitates-I. Normal grain growth”, Acta Metall. et Mater., 43 (1995) 2673-2688.

[34] S.C. Cifuentes, M.A. Monge, P. Pérez, “On the oxidation mechanism of pure tungsten in the temperature range 600–800 °C”, Corrosion Science 57 (2012) 114-121.

[35] H. Pinch, B. Abeles, J.I. Gittleman, “ Method of making high resistance cermet film”, US Patent 4010312, March, 1977.

Figure captions

Fig. 1- a) Reflectance of Tungsten layers deposited on polished and of polished stainless steel substrates; b) n and k of Tungsten layers

Fig. 2- Refractive index (n) and extinction coefficient (κ) of Al_2O_3:W layers as a function of the wavelength.

Fig. 3- Representative RBS spectra of two different Al_2O_3:W thin films, with W volume fractions of 0.18 and 0.34.

Fig. 4-XRD patterns of single layers performed with an incidence angle of 3º of: a) Al_2O_3:W cermet layers deposited on polished stainless steel, where f represents the W volume fraction and b) AlSiN and AlSiON layers, deposited on glass.

Fig. 5- Sketches of multilayers based on Al_2O_3:W cermets (CM1 and CM2) and AlSiN/AlSiON layers (SAON1 and SAON2), where are indicated the thicknesses of the layers and the metal volume fraction in case of Al_2O_3:W cermets.

Fig. 6- Reflectance of a four layers stack deposited on stainless steel substrates. The solar absorptance and thermal emittance (calculated for 400 ºC) of different coatings are also indicated in the legend.

Fig. 7- Fractured cross section SEM images of (a) CM1 (W/Al_2O_3:W(f=42%)/Al_2O_3:W(f=23%)/SiO_2) and (b) SAON1 (W/AlSiN/AlSiON/SiO_2) samples deposited on stainless steel substrates. The bottom layer corresponds to W layer, and the top layer to the antireflection layer. The intermediate layer corresponds to the double layer structure (HA and LA layers), not resolved in figure.

Fig.8 - Reflectance of CM1 coating, in as deposited state and after thermal annealing in air (a) and vacuum (b), as indicated in the figure. The solar absorptance and thermal emittance (at 400 ºC) after each step are also indicated in the figure.

Fig.9 - Reflectance of coatings: a) CM2 and b) SAON1, in as deposited state and after thermal annealing in air and vacuum, as indicated in the figure. The solar absorptance and thermal emittance (at 400 ºC) after each step are also indicated in the figure.

Fig.10 - X-Ray patterns of samples CM1 (a) and SAON1 (b) measured in as deposited state and after thermal treatments, as indicated in the figure. The legend indicates the difractograms from bottom to top.

Fig. 11- Solar absorptance and emissivity (calculated for 400 ºC) as a function of the annealing time: a) at 400 ºC in air and b) at 580 ºC in vacuum for different coatings, as indicated in the figure. The lines were introduced only to guide the eyes.

Table

Table 1 – Deposition parameters of individual layers used to build the multilayer stack. I_1 represents the current density on W target and I_2 the current density on Al and Al(Si) targets

Layer denomination	p_{Ar} [Pa]	p_{O2} [Pa]	p_{N2} [Pa]	rot (rpm)	I_1 [A/cm^2]	I_2 [A/cm^2]	deposition rate [nm/s]
W (static)	0.45	-	-	-	1.3E-2	-	1.3
HA Al_2O_3 (vol. fract. 42% W)	0.45	0.035		15	8.3E-3	6.4E-3	0.4
LA:Al_2O_3 (vol. fract. 23% W)	0.45	0.035	-	15	3.2E-3	6.4E-3	0.3
HA:$Al_{2.5}SiN_y$	0.45	-	0.026	-	-	6.4E-3	0.9
LA: $Al_{2.5}SiO_xN_y$	0.45	0.0056	0.032	-	-	6.4E-3	0.6
HA:$Al_{2.5}SiN_y$	0.45	-	0.023	15	-	6.4E-3	0.2
LA: $Al_{2.5}SiO_xN_y$	0.45	0.0051	0.029	15	-	6.4E-3	0.2
AR: Al_2O_3 or $AlSi_{1.3}O_x$	0.45	0.035	-	15	-	6.4E-3	0.1

Fig. 1- a)

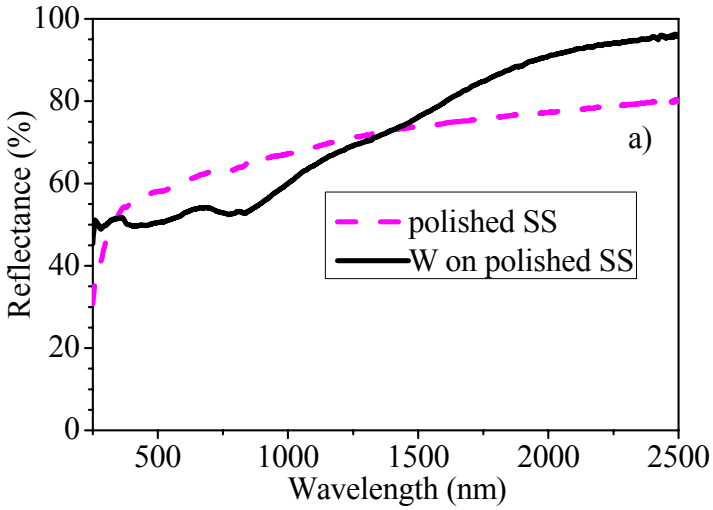

Fig. 1- b)

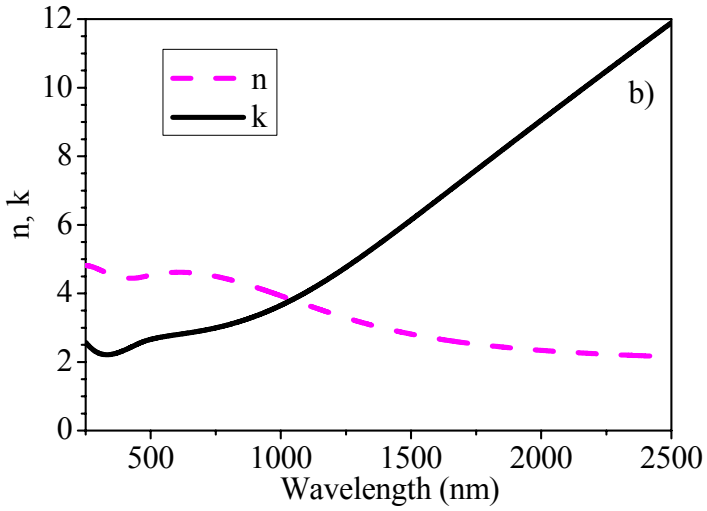
n
k
b)
n, k
Wavelength (nm)

Fig. 2

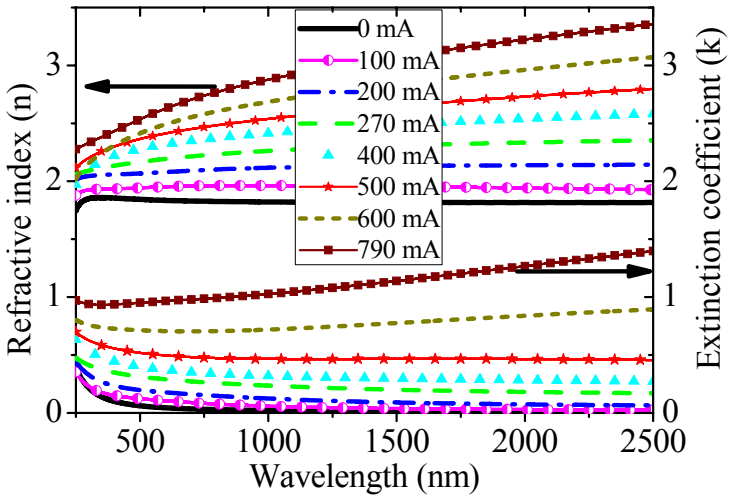
0 mA
100 mA
200 mA
270 mA
400 mA
500 mA
600 mA
790 mA
Refractive index (n)
Extinction coefficient (k)
Wavelength (nm)

Fig. 3

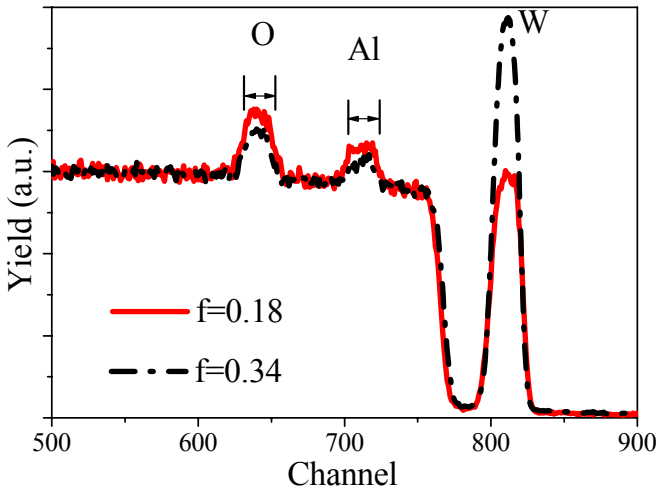
O
Al
W
Yield (a.u.)
f=0.18
f=0.34
500
600
700
800
900
Channel

Fig. 4- a)

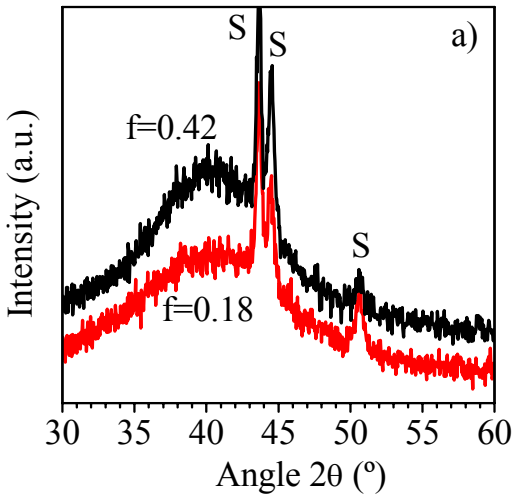
S
S
a)
f=0.42
S
f=0.18
Intensity (a.u.)
30
35
40
45
50
55
60
Angle 2θ (º)

Fig. 4- b)

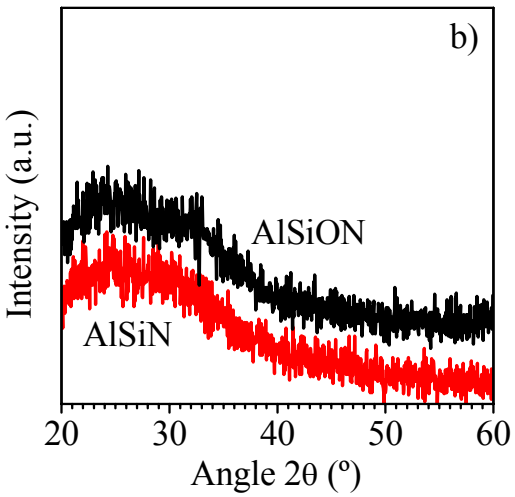
b)
Intensity (a.u.)
AlSiON
AlSiN
20
30
40
50
60
Angle 2θ (º)

Fig. 5

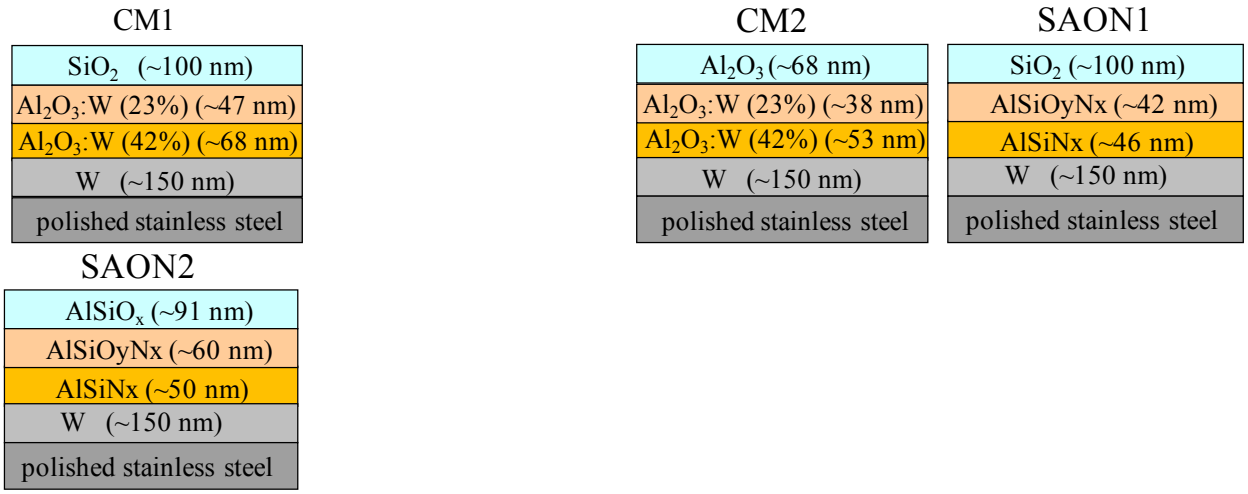
CM1
SiO2 (~100 nm)
Al2O3:W (23%) (~47 nm)
Al2O3:W (42%) (~68 nm)
W (~150 nm)
polished stainless steel
SAON2
AlSiOx (~91 nm)
AlSiOyNx (~60 nm)
AlSiNx (~50 nm)
W (~150 nm)
polished stainless steel
CM2
Al2O3 (~68 nm)
Al2O3:W (23%) (~38 nm)
Al2O3:W (42%) (~53 nm)
W (~150 nm)
polished stainless steel
SAON1
SiO2 (~100 nm)
AlSiOyNx (~42 nm)
AlSiNx (~46 nm)
W (~150 nm)
polished stainless steel

Fig. 6

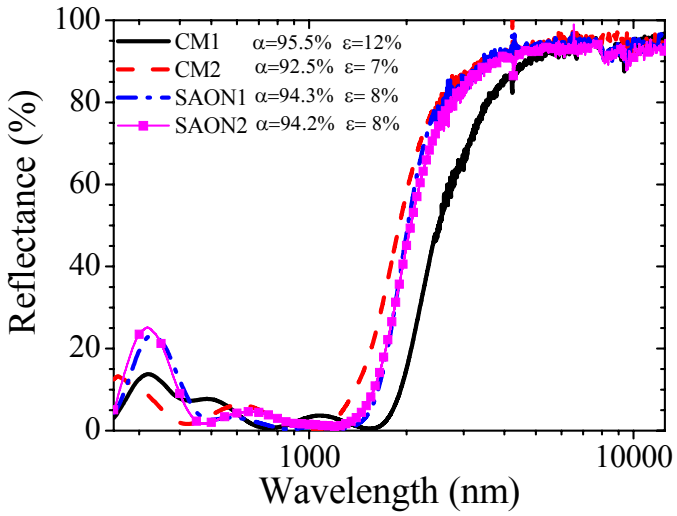
CM1 α=95.5% ε=12%
CM2 α=92.5% ε= 7%
SAON1 α=94.3% ε= 8%
SAON2 α=94.2% ε= 8%
Reflectance (%)
Wavelength (nm)
100
80
60
40
20
0
1000
10000

Fig. 7 – a)

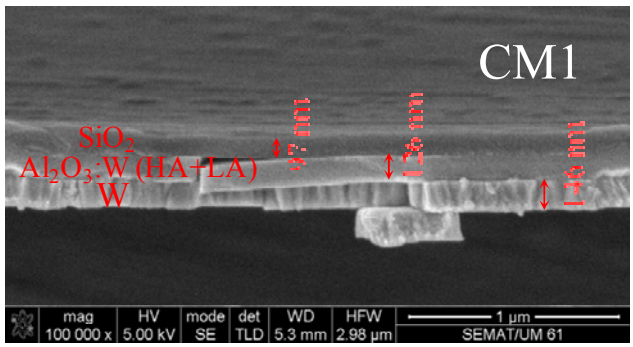
CM1
SiO2
Al2O3:W (HA+LA)
W
mag
HV
mode
det
WD
HFW
1 µm
SEMAT/UM 61

Fig. 7 – b)

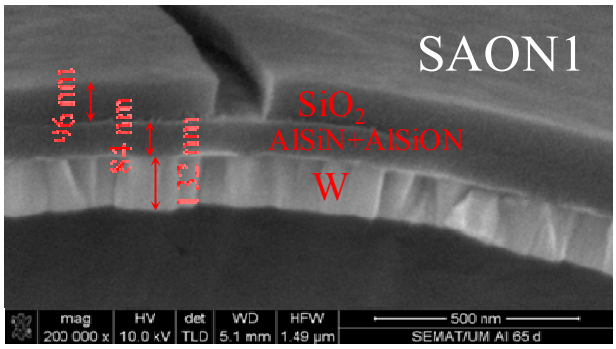
SAON1
SiO2
AlSiN+AlSiON
W
mag
HV
det
WD
HFW
500 nm
SEMAT/UM Al 65 d

Fig. 8 – a)

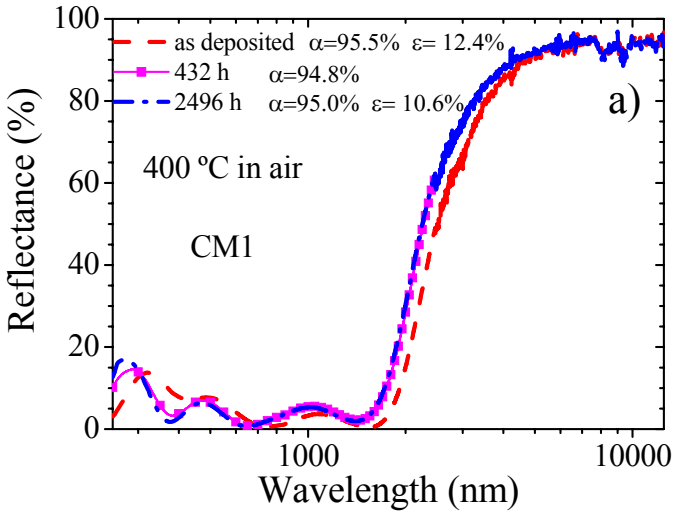

Fig. 8 – b)

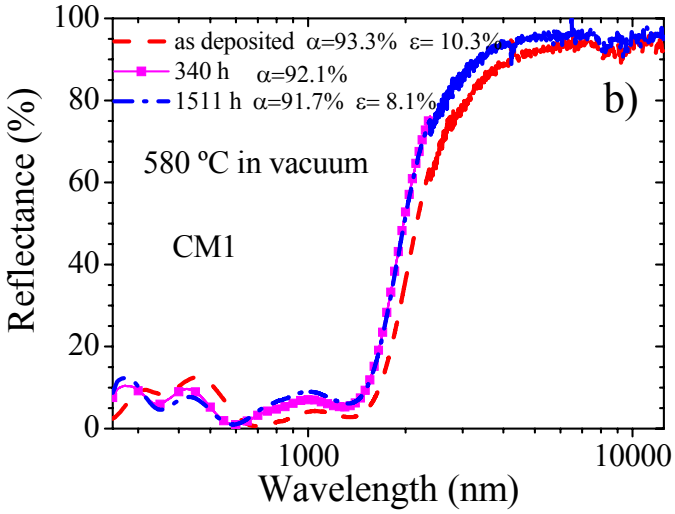

Fig. 9 – a)

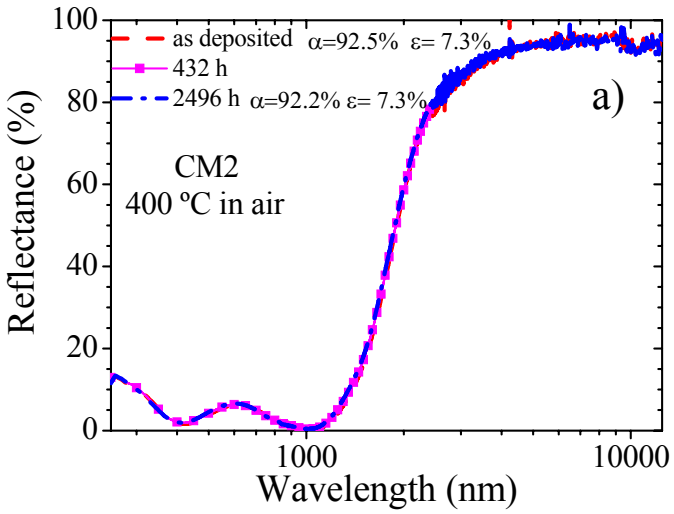
as deposited α=92.5% ε= 7.3%
432 h
2496 h α=92.2% ε= 7.3%
a)
CM2
400 ºC in air
Reflectance (%)
Wavelength (nm)
100
80
60
40
20
0
1000
10000

Fig. 9 – b)

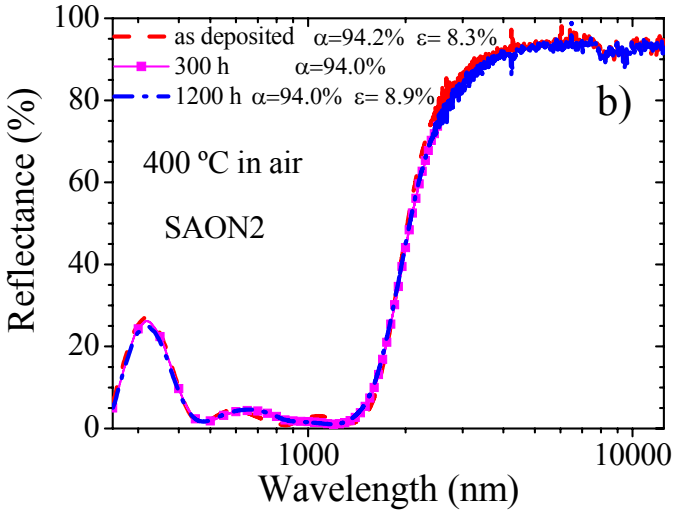
as deposited α=94.2% ε= 8.3%
300 h α=94.0%
1200 h α=94.0% ε= 8.9%
b)
400 ºC in air
SAON2
Reflectance (%)
Wavelength (nm)
100
80
60
40
20
0
1000
10000

Fig. 10

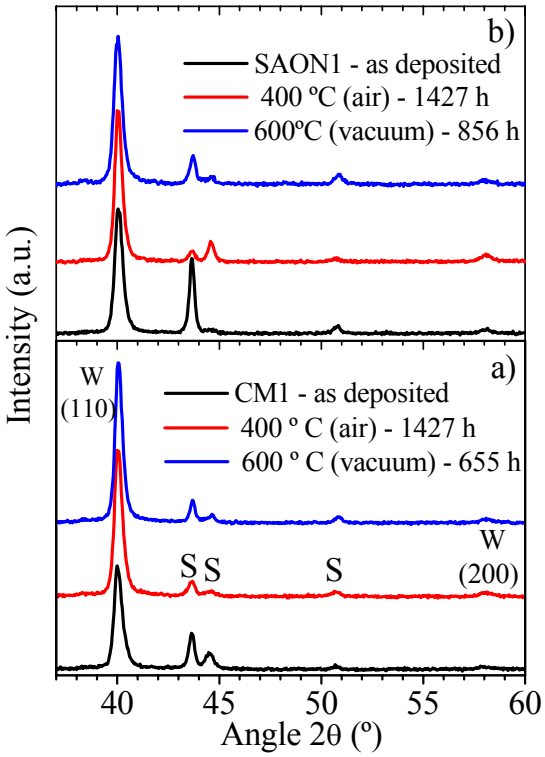
b)
SAON1 - as deposited
400 ºC (air) - 1427 h
600ºC (vacuum) - 856 h
Intensity (a.u.)
W
(110)
a)
CM1 - as deposited
400 º C (air) - 1427 h
600 º C (vacuum) - 655 h
S S
S
W
(200)
40
45
50
55
60
Angle 2θ (º)

Fig. 11 – a)

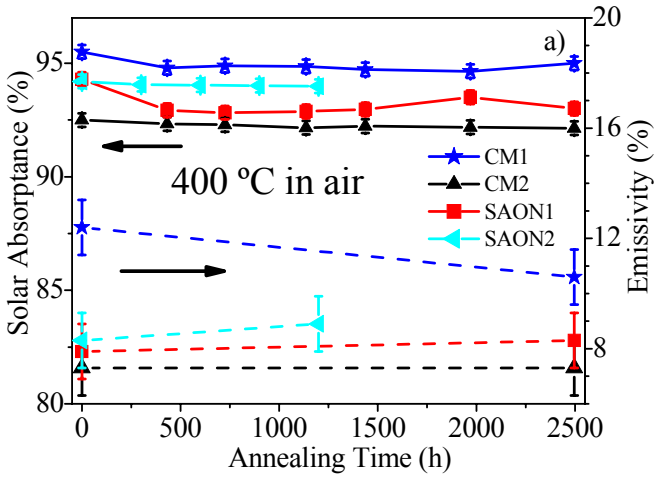

Fig. 11 – b)